Chemistry Africa (2025) 8:5453–5462
https://doi.org/10.1007/s42250-025-01389-8

ORIGINAL ARTICLE

Cellulose Acetate Reinforced with Acetylated Nanocellulose Fibres

Christopher D. Denton[1] · Walter W. Focke[1] · Shatish Ramjee[1] · James Wesley-Smith[2]

Received: 16 February 2025 / Accepted: 13 July 2025 / Published online: 22 August 2025

Abstract
Surface acetylation of cellulose nanofibers (CNFs) was investigated to enhance compatibility with triacetin-plasticized cellulose diacetate (CA). This modification reduced fibre agglomeration, doubling the Young's modulus at the 15% loading, though tensile strength remained largely unchanged.

Keywords Cellulose acetate; Cellulose nanofiber; Acetylation; Composite cellulose acetate · Acetylated nanocellulose · Triacetin plasticiser · Young's modulus · Tensile strength · Biodegradable composites · Surface modification

1 Introduction

Petroleum-based plastics play an important role in almost every aspect of human life however, due to the non-existent biodegradability of these materials, their production and use has a detrimental effect on the environment. It was found that microplastics are even accumulating inside living creatures, eliciting major adverse health effects [1]. Biodegradable polymers potentially offer a partial solution to the problem posed by conventional plastics. However, they come with their own set of problems. Cellulose acetate (CA), a polymer based on the cellulose fibres found in plants, could replace a portion of the plastics market [2]. Unfortunately, it falls short in terms of certain mechanical properties.

Cellulose forms a crucial part of the cellular structure, imparting strength and rigidity to the plant [3]. As one of the most abundant naturally occurring, biodegradable materials it is mostly exploited by the pulp and paper industry. Beyond the classic applications, this industry is exploring further refinement of cellulose into a new form, e.g. nanocellulose [4], with cellulose nanofibres (CNFs) being particularly interesting. CNFs are highly refined cellulose fibres with diameters in the nanometre range. They form interconnected webs which can greatly improve properties of a polymer matrix such as, tensile strength. Currently, the major applications of CNFs are in the cosmetic and construction industry where its shear-thinning behaviour provides advantages [5, 6]. CNFs are typically supplied as water-based suspensions containing as little as 8% solids [7]. When this product is dried, it undergoes hornification, an irreversible agglomeration of the cellulose fibres due to the formation of interchain hydrogen- and hemiacetal bonds (lactone bridges) [8]. Although hornification can be avoided through certain drying methods however these methods are rather energy intensive [9].

Incorporation of CNFs into triacetin-plasticised CA yields has been shown to improve its mechanical properties. This in spite of some loss in the degree of fibrillation of the cellulose fibres which hampers the reinforcement from CNFs [10]. This can be attributed to the mismatch in the composition of the matrix and the filler. The CNFs preferentially agglomerate rather than be wetted by the matrix material, leading to the present research question: Can the compatibility of the constituents be improved by acetylating the CNFs surfaces [11]? This approach has proved promising in PLA, another biodegradable polymer, with a good fibre dispersion due to the non-polar nature of the matrix [12]. In order to acetylate the CNFs, acetic anhydride is used to react with the surface hydroxyl groups, converting them into acetyl groups [13]. However, this approach poses two challenges, the first of which relates to the high moisture content of the CNFs as supplied. Acetic anhydride preferentially reacts with water to form acetic acid instead of acetylating the CNFs. Furthermore, water has to be

✉ Walter W. Focke
walter.focke@up.ac.za

[1] Department of Chemical Engineering, University of Pretoria, Lynnwood Rd, Pretoria, Gauteng 0028, South Africa

[2] Empower Microscopy, 273 Driehoek Street, Pretoria, South Africa

removed without collapsing the fibre network, due to hornification, but this can be done through azeotropic distillation [14]. Recent studies have shown that a solvent swap can be done by simply adding xanthan gum to the CNFs [15]. This maintains the network during drying and allows redispersion of the CNF in acetic acid. The second problem relates to the degree of acetylation of the cellulose fibres. This factor indicates the fraction the hydroxyl groups per monomer which was replaced. If the acetic anhydride attacks the linking oxygen between the cellulose monomers, instead of the hydroxyl groups, the long polymer chains are shortened and cellulose nanocrystals form [16]. However, if these factors are carefully controlled, it could lead to an acetylated fibrous material that can be easily dispersed in a CA matrix. This should result in improvements in the tensile strength and Youngs modulus and even in the optical transparency. These were the objectives explored in the present study.

2 Experimental

2.1 Materials

Cellulose diacetate (Batch number HH20191010) was supplied by Haihang Industry Co., China. Sappi Southern Africa Technology Centre supplied the CNF (Valida S191C 8%, Batch SB-20-0126-01). The actual solids content of this suspension was 8.2 wt%. Solvent acetic anhydride (purity≥98.5%) and plasticizer triacetin (99%) were sourced from Merck South Africa, Modderfontein, South Africa. Chemically pure acetone, acetic acid and sulphuric acid were purchased from Acechem, Johannesburg, South Africa.

2.2 Methods

2.2.1 Acetylation of Cellulose Nanofibres

Before use, the CNF was kept stored at a temperature of 4 °C. Every CNF modification was done in the same way except that the relative amount of acetic anhydride employed was varied to control the degree of substitution (DS) of the CNF, i.e. the number hydroxyl groups, on the cellulose repeat units, potentially converted into acetyl groups. The quantity of acetic anhydride used, corresponded to four DS values for complete conversion, i.e. 0, 0.5, 1 and 1.5. However, the CNF is a highly crystalline material and it is unlikely that such a complete (and undesirable) conversion would be achieved. Rather, the excess reagent quantities were selected to drive the degree of surface modification to a limiting value.

To remove the water present in the pulp 30 g of the raw CNF was weighed out and dispersed in 150 mL of glacial acetic acid. The mixture was mixed for a minute and then agitated with a Silverson L4RT high shear mixer at 2000 rpm for 2 min. The azeotropic distillation that followed entailed agitating the suspension using magnetic stirring at a speed of 500 rpm and the mixture was gradually heated. The solvent removal was interrupted when the temperature of the mixture reached 120 °C. An additional amount of acetic acid (50 mL) was added and the distillation continued for a further 20 min. A spatula sized sample of the suspension was weighed and put aside for analysis, including the determination of the solids content. The remainder of the paste was stored in a sealed jar and used as the base material for the acetylation reaction.

Each batch acetylation was performed using 20 g of this base material placed in a 250 mL beaker with 100 mL of acetic acid and then high-shear mixed at 2000 rpm for 1 min at room temperature. The beaker was stirred at 400 rpm using a magnetic stirrer and gradually heated to 60 °C, upon which 50 µL of sulphuric acid was slowly added over a period of 10 min. The desired amount of acetic anhydride was calculated based on the measured solids content of the particular batch, and added to the mixture. The mixture was allowed to react for four hours, after which 50 mL of deionized water was slowly poured into the mixture to arrest the acetylation reaction. The solution was vacuum filtered and washed with acetic acid before being labelled and stored at 4 °C. A small sample was taken to determine the final solids content of the acetylated paste. The only concern for this method is to ensure that the distillation step is followed otherwise results will not be reproducible.

2.2.2 Cellulose Acetate Film Preparation

All films were made using a casting method with the triacetin used as the plasticizer. The plasticizer content, based on the cellulose acetate (CA) amount, was held constant at 25 wt%. For each acetylated CNF sample, four films differing in the CNF content were cast, namely 2, 5, 10 and 15% relative to the CA content. The films were labelled according to the format: "C*DS#" where "*" represents the percentage CNF and "#" represents the value for the targeted DS. A control film, which contained no CNF, was labelled "Pure". The films were made as follows. First the adjusted amount of paste, corresponding to the desired CNF amount to modify 1 g of CA, was weighed into a beaker. Next, 50 mL of acetone was added, and the contents stirred to loosen and homogenise the paste. Then the mixture was subjected to high shear for 2 min in a Silverson L4RT mixer operating at 1500 rpm. At this stage, 1.00 g CA and 0.33 g triacetin were added. The mixture was then shear-mixed in the Silverson

at 2500 rpm for 3 min. This was done to ensure good dispersion of the CNF. During this mixing process, some air was entrained owing to the high viscosity of the dispersion. The trapped air was removed using a vacuum chamber. Three consecutive depressurizing cycles were applied. In these, the chamber pressure was reduced to 0.4 bar, left for 1 min, and then slowly repressured back to atmospheric pressure. The resulting mixture was then poured into a Petri dish (80 mm φ) and left overnight in a fume hood to allow the acetone to evaporate slowly. For the films with the highest CNF content, it proved necessary to half-cover the Petri dishes in order to slow the rate of evaporation. This intervention prevented unwanted warping of the films. The dried films were removed from the Petri dishes and the edges were trimmed with scissors. The final film thicknesses were approximately 130 µm. The films were labelled and placed in an airtight box containing a saturated NaCl solution and maintained at a temperature of 20 °C. This means that the films were conditioned at a relative humidity (RH) of 76% [17].

2.3 Characterisation

2.3.1 Fourier Transform Infrared (FTIR)

Fourier transform infrared spectra (FTIR) were recorded with a Perkin Elmer Spectrum 100 FTIR Spectrometer fitted with an attenuated total reflectance (ATR) attachment. The reported spectra represent the average 32 scans taken in the range of 4000 cm^{-1} to 650 cm^{-1} at a resolution of 4 cm^{-1}.

2.3.2 Thermogravimetric Analysis (TGA)

Thermogravimetric Analysis (TGA) was performed on a TA instruments TGA 5500. Samples, weighing ca. 5 mg, were placed either in alumina (Al_2O_3) crucibles or in high-temperature platinum pans. The temperature was scanned from 30 °C to 800 °C at a rate of 20 °C min^{-1} in a nitrogen (N_2) atmosphere.

2.3.3 X-ray Diffraction (XRD)

The X-ray diffraction (XRD) diffractograms were captured on a Malvern Panalytical Aeris diffractometer with a PIXcel detector and fixed slits. Fe-filtered Co-Kα radiation (λ = 0.1789 nm) was used with a back-loading preparation and zero background holder method. Scans were taken from 5° to 80° 2θ at 0.02° s^{-1}.

2.3.4 Transmission Electron Microscopy (TEM)

Transmission Electron Microscopy (TEM) images were obtained using a JEOL JEM 1400 Flash at 100 kV. The CNF was contrasted using 0.5% aqueous uranyl acetate as a negative stain. A 5 µL drop of diluted CNF solution was placed on one side of a carbon-coated Formvar TEM grid and allowed to stand for 30 s, before placing (droplet side down) on a 5 µL droplet of uranyl acetate. After 15 s, excess liquid was removed using filter paper and the grids were allowed to air dry before TEM imaging.

2.3.5 Light Microscopy

Films were imaged at 1000× magnification on a Motic DMB1-223 light microscope and the pictures were edited using MotiConnect v1.0.1.9 software.

2.3.6 Mechanical Testing

Mechanical properties of the films were determined on an Instron 5966 universal testing system according to the ASTM D882-18 Standard. The grip separation was 40 mm and an extension rate of 10 mm min^{-1} was applied. The test pieces were obtained using a custom, 3D printed, dog-bone punch licensed from Print-A-Punch [18]. The blades were replaced after every five samples to ensure clean cuts through the film samples. For each formulation, seven separate dog-bone samples were tested. The film thickness, used for calculations, was the average of three measurements taken at different positions along the length of the test pieces. The average film thickness, taken over all the samples tested, was 115 µm with a standard deviation of 10 µm.

3 Results and Discussion

3.1 Fourier Transform Infrared (FTIR)

Figure 1 shows the FTIR spectra, for the CNF-cellulose acetate films, in the range 1300 cm^{-1} to 1900 cm^{-1}. The band located at 1640 is due to O-H bending vibrations and it is present in all three films. The band located at 1720 reflects carbonyl stretching vibrations in the acetyl groups. As expected, this band is absent in the neat nanocellulose sample. It appears as a shoulder in the DS = 0.5 and as well-defined peaks in the other samples. As anticipated, the relative intensity of this band increased with the increase in the nominal DS values of the CNF samples. This suggests successful acetylation of the CNFs surfaces.

3.2 Transmission Electron Microscopy (TEM)

Figure 2 shows TEM images for the various CNF samples. They represent the appearance of the CNFs in the fully dried, possibly hornified, state [19]. The images show the

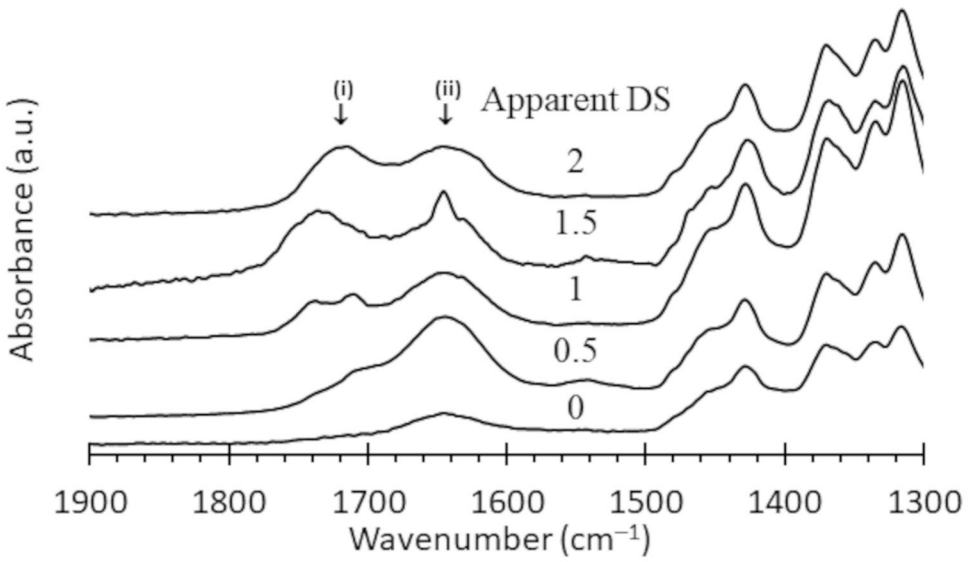

Fig. 1 FTIR spectra of the CNF samples compared to the spectrum of a cellulose acetate film. (i) reflects Carbonyl stretching vibrations (1720 cm^{-1}), and (ii) O-H bending vibrations in the acetyl groups (1640 cm^{-1})

presence of networks of fibrous strands with diameters in the sub-micron range. The staining revealed that these strands comprise long bundles of much finer, well-aligned filaments with lateral dimensions in the nanometre range. In principle the staining helps to ascertain the individual fibre diameters in the bundles [20]. The staining appears to be more intense in the higher-level acetylated CNF samples suggesting weaker interactions between the fibrous strands making up the bundles. This is seen from the greater contrast between black and white regions appose to the more homogenous grey regions indicative of the lower level of acetylation.

3.3 X-ray Diffraction (XRD)

Figure 3 shows the XRD results for the modified CNF samples and for the films loaded at different levels prepared with the DS = 1 CNF. Figure 3(a) shows that the results for the various CNF samples are very similar, i.e. that the basic structure of the cellulose was not affected by the acetylation. The reflection located at 28° is consistent with Type I_β cellulose. Two dominant reflections, contributed by the polymer matrix, are in evidence in the composites. The first is located at 8° and it relates to the van der Waals halo. The second is located at around 22° consistent interplanar distance of 11.1 Å in crystalline CA domains [21]. Figure 3(b) shows, as expected, that the CNF reflections become more prominent as the loading of the reinforcement increases.

3.4 Thermogravimetric Analysis (TGA)

Figure 4 shows the TGA mass loss curves for the neat CA and composites prepared using the DS = 1 CNF. The mass loss curves for the CA10DS1 and CA15DS1 composites practically coincided. This was also the case, up to about 220 °C, for the TGA traces of the other samples. However, above this temperature, the TGA traces deviate from each other. Rapid mass loss is observed but similar mass loss plateaus apply to all samples from about 400 °C and higher. In the intermediate temperatures, the mass loss was higher for composites with higher CNF loadings. The implication is that the presence of the CNF reinforcement accelerated the volatilisation of the plasticized cellulose acetate matrix. This is supported by previous research [10]. Nevertheless, these results do not raise concerns about the viability of the use CNF in plasticized CA as stability in the typical application range is not affected [22].

3.5 Optical Light Microscopy (OM)

Figure 5 compares OM images at 1000 X magnification of two composite films containing 15% CNF. Figure 5(a) shows the composite made using unmodified CNF while Fig. 5(b) shows the corresponding composite based on the DS = 1.5 CNF. Both images show good dispersion of the fibrous CNF reinforcement. The only difference is in the thicknesses of the fibres. They are up to 30 µm in Fig. 5(a) and mostly less than 8 µm in Fig. 5(b). Considering the TEM images in Fig. 1, it is clear that these higher fibre diameters indicate that considerable agglomeration happened when the composites were prepared. However, the significantly smaller CNF diameters observed for the surface-modified material suggest that it reduced the tendency for hornification.

3.6 Mechanical Testing

Table 1 shows the effect of the degree of surface modification and the CNF loading level on the Young's modulus.

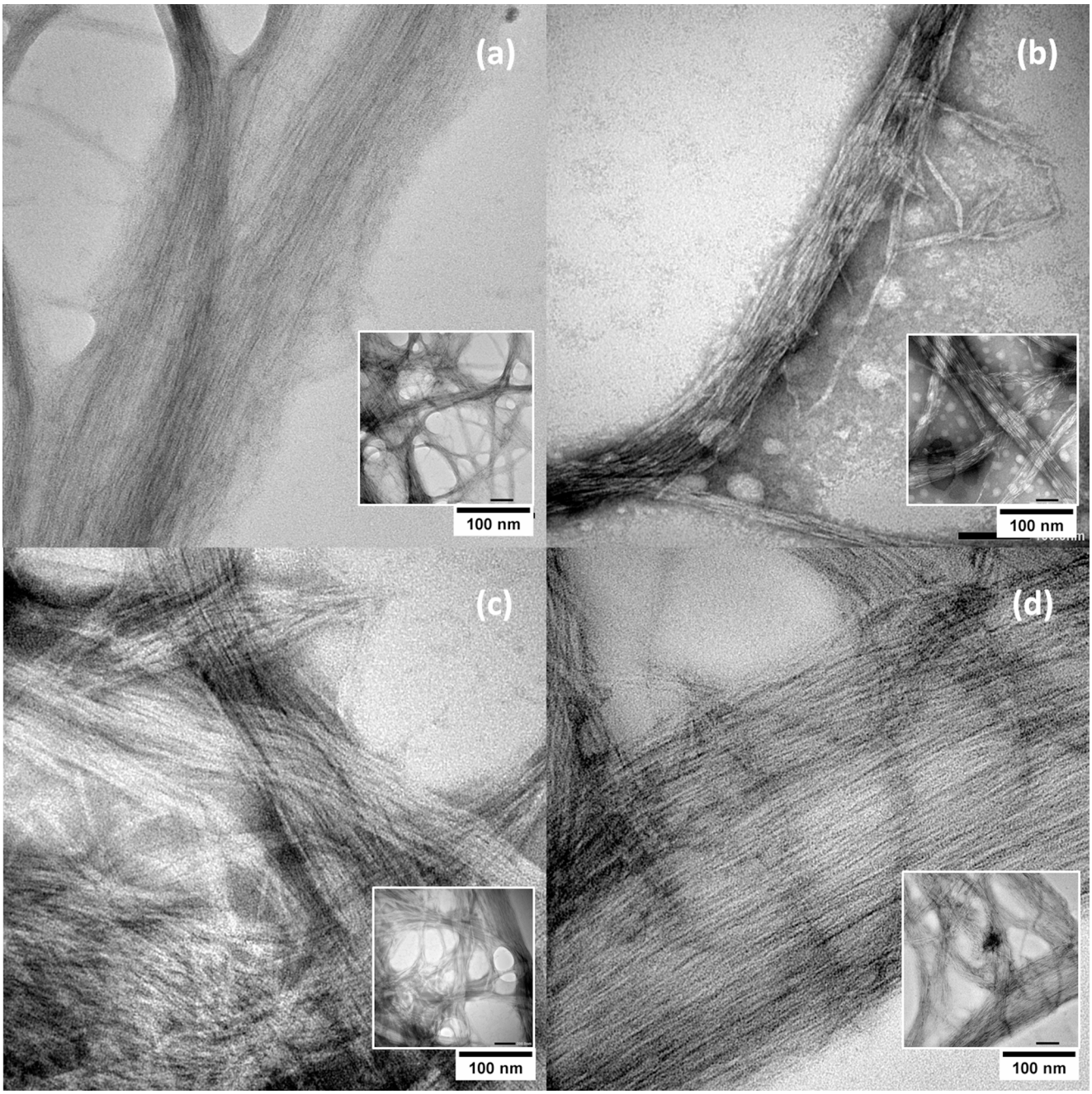

Fig. 2 TEM images of the nanocellulose samples. (**a**) Neat nanocellulose; (**b**) DS = 0.5; (**c**) DS = 1.0, and (**d**) DS = 1.5. The small inserts show images that cover a greater sample area and the indicated scale bars in them also show a length of 100 nm

Table 2 shows the corresponding tensile strengths. Unfortunately, there is a lot of scatter in the present data as indicated by the high standard deviations. This is suspected to be due to drying conditions varying over the dryer area. Nevertheless, it can be stated with confidence that the reinforced sample featured higher elastic moduli and strengths compared to the neat plasticised cellulose material. It seems that that degree of acetylation of the CNF did not appear to have a statistically significant effect on the measured tensile strength of the films due to the large standard deviation in results. For the present samples, the highest tensile strength improvements, by 50%, was achieved with the unmodified CNF also at a loading of 15% as well as at DS = 1.5 CNF loaded at 2%. Best stiffness improvement, by a factor of nearly two, was obtained with the DS = 0.5, CNF loaded at 15%. If only the composites containing 15% CNF are considered, it would appear that there might be an optimum surface modification level, near DS = 0.5, if improvements in

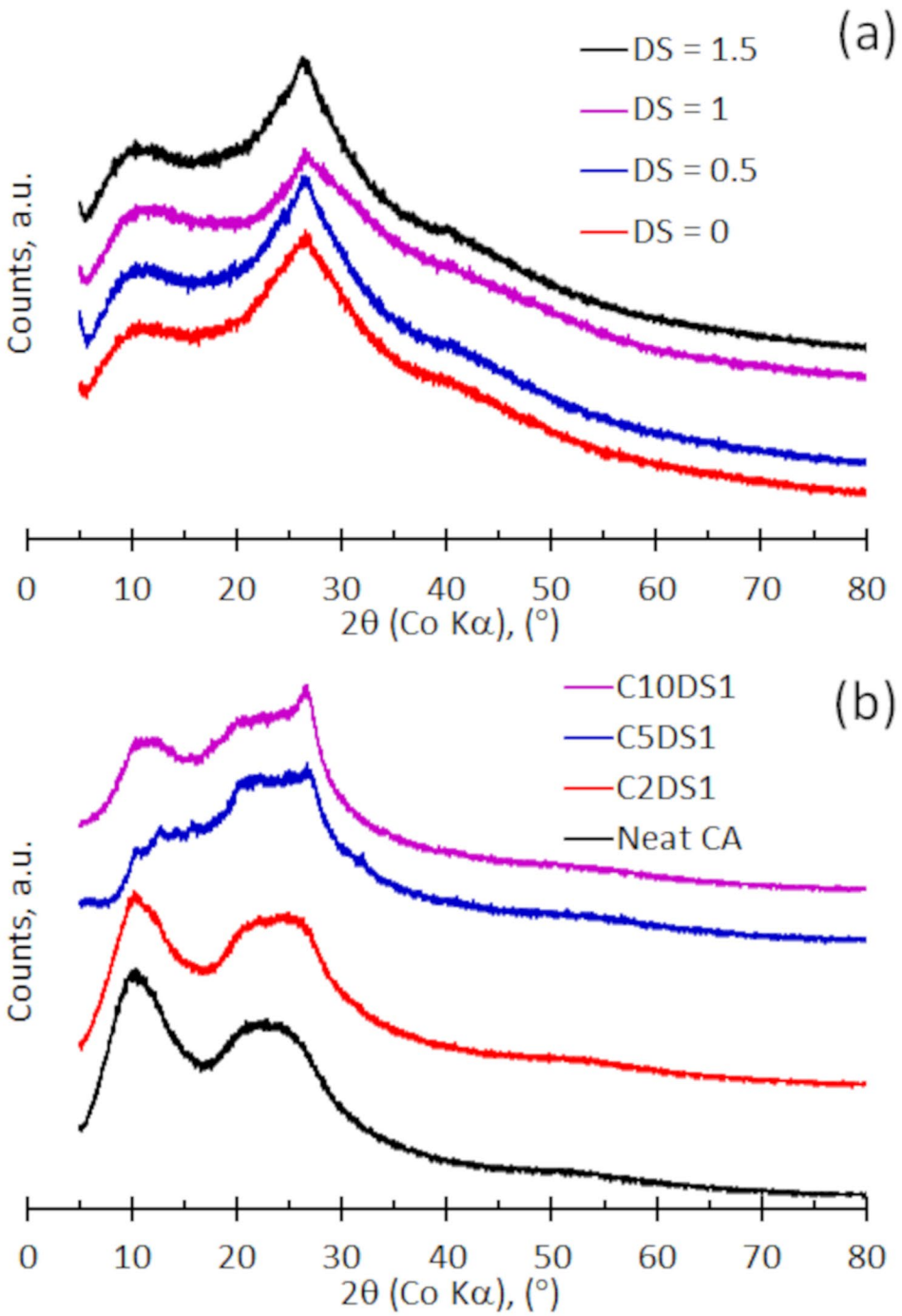

Fig. 3 UV-Vis spectra images of the nanocellulose samples. (**a**) Neat nanocellulose; (**b**) DS = 0.5; (**c**) DS = 1.0, and (**d**) DS = 1.5

the Young's modulus are the focus. If true, a rationalisation of this result could be made on the matching of the surface energy of the CNF fibres with the physiochemical properties of the matrix as determined by the degree of substitution of the polymer and the effect of the plasticiser.

The present mechanical property improvements may be put in perspective by comparing them to results obtained by others. Cindradewi et al. [10] also studied cellulose acetate plasticized with 30 wt% triacetin and reinforced with cellulose nanofibrils. At the highest fibre loading (9 wt%), they found increases in elastic modulus and tensile strength of 65% and 38%. Kouaja et al. [23] studied cellulose acetate plasticized with 30 wt% triethyl citrate and reinforced with microcrystalline cellulose. They found that incorporating 50 wt% cellulose fibres increased the Young's modulus of the plasticized polymer matrix by 300% and the tensile strength by just 12%. Acarer-Arat et al. [24], and Attari et al. [25] reported on the mechanical properties of plasticizer-free

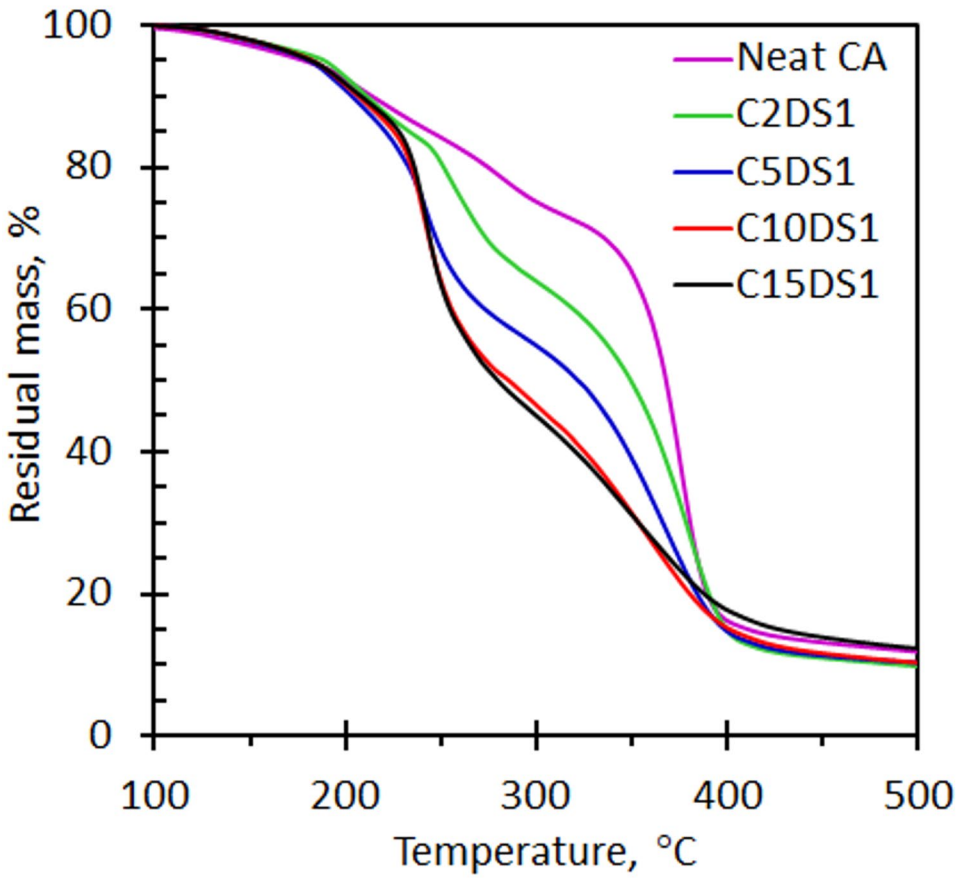

Fig. 4 Thermogravimetric analysis of films. The temperature was scanned from 30 °C to 800 °C at a rate of 20 °C min^{-1} in a nitrogen (N_2) flowing at 50 mL min^{-1}

cellulose acetate reinforced with 1 wt% CNF. The former reported increases the modulus and tensile strength by 695% and 108% respectively. Instead, the latter study found improvements of just 33% and 142% respectively. These results suggest that the presence of a plasticizer has a significant influence on the property enhancements that are achievable.

The Halpin-Tsai equation can be used to predict the variation of composite stiffness with the fibre loading [26].

$$\frac{E_C}{E_M} = \frac{1 + c\upsilon_f}{1 - \eta\upsilon_f} \tag{1}$$

With

$$\eta = \frac{\alpha E_f / E_M - 1}{\alpha E_f / E_M + c} \tag{2}$$

In these equations, E_c, E_m and E_f refer to the moduli of the composite, the neat polymer and fibre reinforcement respectively; υ_f is the volume fraction of the fibre in the composite; c is a shape fibre factor, and α pertains to the fibre orientation factor. The shape factor is further described as

$$c = \frac{2L}{d}\exp(a\upsilon_f - b) \tag{3}$$

where L and d represent the length and diameter of the fibres while a and b are constants which account for the agglomeration of the CNF [27]. Here the orientation factor is taken as one third due to the random orientation and high fibre aspect ratio as explained in [28]. The modulus from the neat sample above is used while the modulus for pure CNF was taken as 115 GPa [29]. Figure 6 compares the predicted Halpin-Tsai data trend with results obtained for the films with the DS = 1 CNF-based composites with $a = 8$ and $b = 0.5$. While the experimental data for this sample appear reasonable, this is not the case for the other samples. There are a number of possible reasons. They include a mismatch in the surface properties of the CNF with respect to the matrix and agglomerated fibre bundles, present in the film, acting as stress concentrators [27].

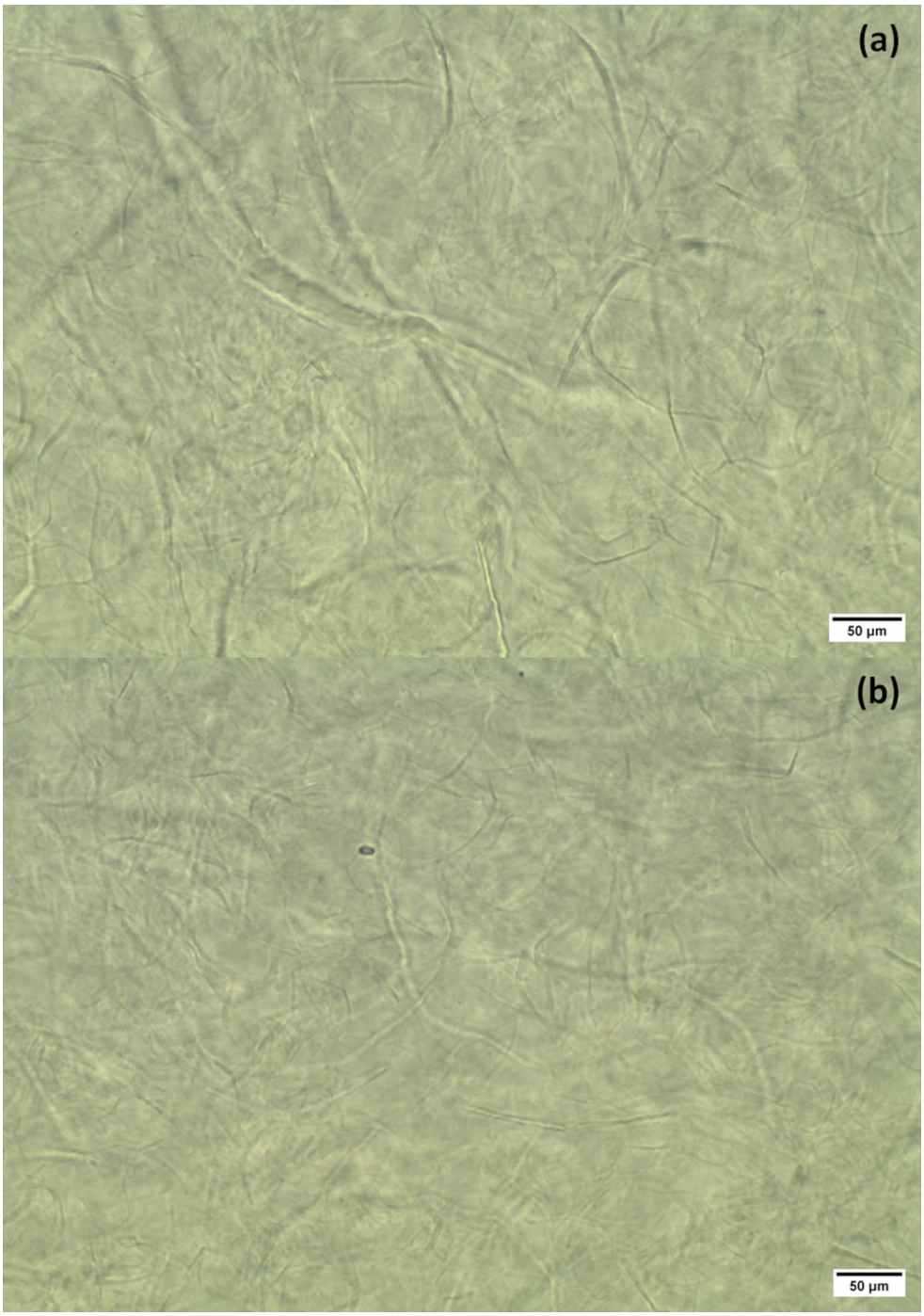

Fig. 5 Optical microscopy images of films reinforced by 15% CNF. (**a**) C15DS0 – no surface modification. (**b**) C15DS1.5 – highest level of acetylation

Table 1 Modulus of elasticity of films (MPa)

CNF Content (%)	Target degree of Substitution			
	0	0.5	1	1.5
0	707±41			
2	987±83	951±82	886±85	1126±175
5	1007±102	908±95	1068±41	1035±80
10	789±76	997±63	1033±53	1069±117
15	952±128	1378±96	1236±30	974±51

Table 2 Tensile strength of films (MPa)

CNF Content (%)	Target degree of Substitution			
	0	0.5	1	1.5
0	36±6			
2	43±5	42±4	43±4	53±11
5	46±4	39±4	45±2	41±2
10	39±4	41±2	40±2	41±3
15	54±3	47±3	46±3	43±3

4 Conclusion

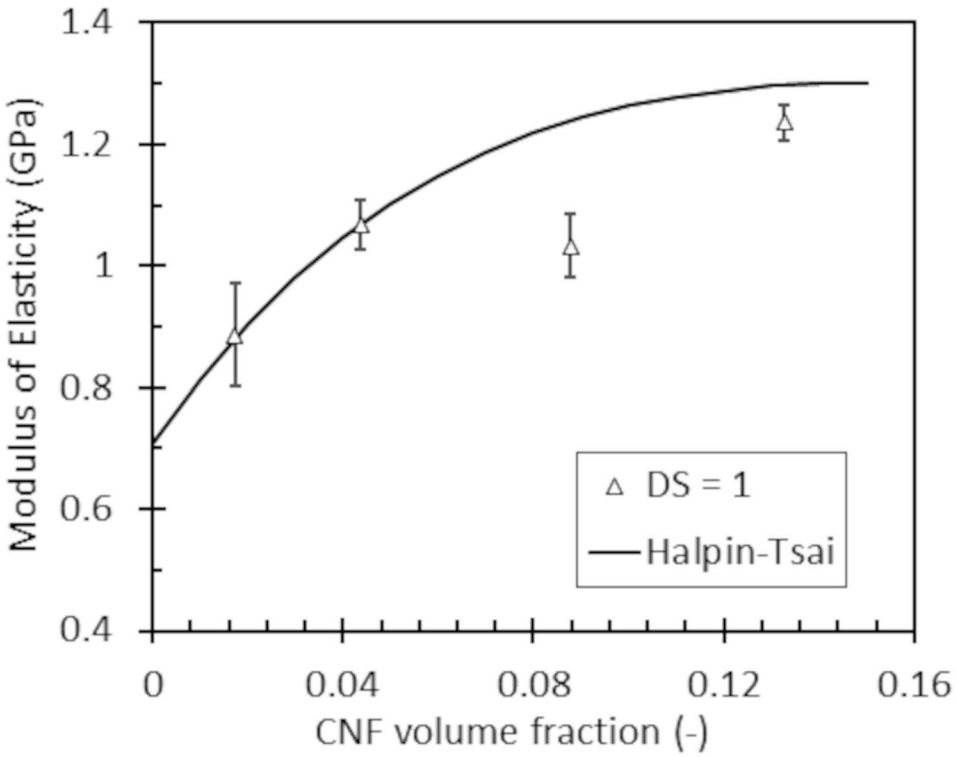

Fig. 6 Comparing the Halpin-Tsai predictions for the Youngs modulus (sold line) with experimental results for the composites prepared with DS = 1 CNF

Cellulose acetate composites (plasticised with 25% triacetin), containing up to 15% cellulose nanofibres, were prepared using a film casting process. Surface acetylation of the cellulose nanofibres was explored as a possible way to reduce their tendency to agglomerate. Fourier transform infrared spectroscopy confirmed successful surface modification, validating the solvent swap method as a viable way to control the degree of substitution. X-ray diffraction studies showed that the cellulose crystal structure was retained. Transmission electron microscopy showed that the tendency of the fibres to agglomerate was reduced. However, optical microscopy revealed that some re-agglomeration did occur during the film casting process. The degree of acetylation did not significantly affect the tensile strength of the composites which can limit the polymer in certain uses and requires further development to overcome this issue. However, at a loading of 15% with acetylated cellulose nanofibres, the Young's modulus was double that of the neat polymer matrix. This is a step the right direction and follows the trend of research demonstrating the potential of biodegradable polymers.

Funding Open access funding provided by University of Pretoria. The research leading to these results received funding from the Paper Manufacturers Association of South Africa (PAMSA).

Declarations

Ethical Approval Not applicable.

Informed Consent Not applicable.

Financial interests The authors have no relevant financial or non-financial interests to disclose.

References

1. Wu P, Lin S, Cao G et al (2022) Absorption, distribution, metabolism, excretion and toxicity of microplastics in the human body and health implications. J Hazard Mater 437:129361. https://doi.org/10.1016/j.jhazmat.2022.129361
2. Carraher CE Jr, Sperling LH (2012) Polymer applications of renewable-resource materials. Springer Science & Business Media, ISBN-13: 978-1461335054
3. Somerville C (2006) Cellulose synthesis in higher plants. Annu Rev Cell Dev Biol 22:53–78. https://doi.org/10.1146/annurev.cellbio.22.022206.160206
4. Dufresne A (2019) Nanocellulose processing properties and potential applications. Curr Rep 5:76–89. https://doi.org/10.1007/s40725-019-00088-1

5. Rajendran N, Runge T, Bergman RD, Nepal P, Nair N, Ashraf W (2025) Economic and environmental impact analysis of cellulose nanofiber-reinforced concrete mixture production. Resour Conserv Recycl 212:107917. https://doi.org/10.1016/j.resconrec.2024.107917
6. Pandey A (2021) Pharmaceutical and biomedical applications of cellulose nanofibers: a review. Environ Chem Lett 19:2043–2055. https://doi.org/10.1007/s10311-021-01182-2
7. Posada P, Velásquez-Cock J, Gómez-Hoyos C et al (2020) Drying and redispersion of plant cellulose nanofibers for industrial applications: a review. Cellulose 27:10649–10670. https://doi.org/10.1007/s10570-020-03348-7
8. Fernandes Diniz JMB, Gil MH, Castro JAAM (2004) Hornification—its origin and interpretation in wood pulps. Wood Sci Technol 37:489–494. https://doi.org/10.1007/s00226-003-0216-2
9. Nordenström M, Kaldéus T, Erlandsson J, Pettersson T, Malmstrom E, Wågberg L (2021) Redispersion strategies for dried cellulose nanofibrils. ACS Sustainable Chem Eng 9:11003–11010. https://doi.org/10.1021/acssuschemeng.1c02122
10. Cindradewi AW, Bandi R, Park C-W et al (2021) Preparation and characterization of cellulose acetate film reinforced with cellulose nanofibril. Polymers 13:2990. https://doi.org/10.3390/polym13172990
11. Ashori A, Babaee M, Jonoobi M, Hamzeh Y (2014) Solvent-free acetylation of cellulose nanofibers for improving compatibility and dispersion. Carbohydr Polym 102:369–375. https://doi.org/10.1016/j.carbpol.2013.11.067
12. Jamaluddin N, Kanno T, Asoh T-A, Uyama H (2019) Surface modification of cellulose nanofiber using acid anhydride for poly(lactic acid) reinforcement. Mater Today Commun 21:100587. https://doi.org/10.1016/j.mtcomm.2019.100587
13. Sassi J-F, Chanzy H (1995) Ultrastructural aspects of the acetylation of cellulose. Cellulose 2:111–127. https://doi.org/10.1007/BF00816384
14. Chien IL, Zeng K-L, Chao H-Y, Liu JH (2004) Design and control of acetic acid dehydration system via heterogeneous azeotropic distillation. Chem Eng Sci 59:4547–4567. https://doi.org/10.1016/j.ces.2004.06.041
15. Hoek Z, du Toit EL, Niemand D, Wesley-Smith J, Focke WW (2024) Dried nanocellulose/xanthan as reinforcing fillers in thermoplastic starch. Cellulose 31:6733–6746. https://doi.org/10.1007/s10570-024-06006-4
16. Miao J, Yu Y, Jiang Z, Zhang L (2016) One-pot Preparation of hydrophobic cellulose nanocrystals in an ionic liquid. Cellulose 23:1209–1219. https://doi.org/10.1007/s10570-016-0864-7
17. Winston PW, Bates DH (1960) Saturated solutions for the control of humidity in biological research. Ecology 41:232–237. https://doi.org/10.2307/1931961
18. Nelson SJ, Creechley JJ, Wale ME, Lujan TJ (2020) Print-A-Punch: A 3D printed device to cut dumbbell-shaped specimens from soft tissue for tensile testing. J Biomech 112:110011. https://doi.org/10.1016/j.jbiomech.2020.110011
19. Peng Y, Gardner DJ, Han Y (2012) Drying cellulose nanofibrils: in search of a suitable method. Cellulose 19:91–102. https://doi.org/10.1007/s10570-011-9630-z
20. Campano C, Balea A, Blanco Á, Negro C (2020) A reproducible method to characterize the bulk morphology of cellulose nanocrystals and nanofibers by transmission electron microscopy. Cellulose 27:4871–4887. https://doi.org/10.1007/s10570-020-03138-1
21. Rodrigues Filho G, da Cruz SF, Pasquini D, Cerqueira DA, de Souza Prado V, de Assunção RMN (2000) Water flux through cellulose triacetate films produced from heterogeneous acetylation of sugar cane Bagasse. J Membr Sci 177:225–231. https://doi.org/10.1016/S0376-7388(00)00469-5
22. Moelter GM, Schweizer E (1949) Heat softening of cellulose acetate. Ind Eng Chem 41:684–689. https://doi.org/10.1021/ie50472a007
23. Khouaja A, Koubaa A, Daly B, H (2025) Mechanical and morphological properties of cellulose biocomposites. Chemosphere 379:144415. https://doi.org/10.1016/j.chemosphere.2025.144415
24. Acarer-Arat S, Pir İ, Tüfekci M, Güneş-Durak S, Akman A, Tüfekci N (2024) Heavy metal rejection performance and mechanical performance of cellulose-Nanofibril-Reinforced cellulose acetate membranes. ACS Omega 9:42159–42171. https://doi.org/10.1021/acsomega.4c03038
25. Attari N, Hausler R (2023) Reinforcing effects of fibrous and crystalline nanocelluloses on cellulose acetate membranes. Carbohydr Polym Tech 5:100281. https://doi.org/10.1016/j.carpta.2023.100281
26. Tucker CL III, Liang E (1999) Stiffness predictions for unidirectional short-fiber composites: review and evaluation. Compos Sci Technol 59:655–671. https://doi.org/10.1016/S0266-3538(98)00120-1
27. Sun L-H, Ounaies Z, Gao X-L, Whalen CA, Yang Z-G (2011) Preparation, Characterization, and Modeling of Carbon Nanofiber/Epoxy Nanocomposites. J Nanomater 2011:307589. https://doi.org/10.1155/2011/307589
28. Cox HL (1952) The elasticity and strength of paper and other fibrous materials. Br J Appl Phys 3:72. https://doi.org/10.1088/0508-3443/3/3/302
29. Zhai L, Kim HC, Kim D, Muthoka RM, Kim J (2018) Young's moduli of cellulose nanofibers measured by atomic force microscopy. Nano-, Bio-, Info-Tech Sensors, and 3D Systems II 10597:104. https://doi.org/10.1117/12.2296836